# RADIATION TOLERANCE OF SINGLE-SIDED MICROSTRIP DETECTOR WITH $Si_3N_4$ INSULATOR

N. Maslov, V. Kulibaba, S. Potin, A. Starodubtsev

*NSC KhIPT, Kharkov, Ukraine*

P. Kuijer, A.P. de Haas

*Utrecht University, The Netherlands*

V. Perevertailo

*SPA 'Detector', Kiev, Ukraine*

***(For ALICE collaboration)***

## 1. Introduction

The ALICE collaboration is investigating the radiation tolerance and operation of silicon microstrip detectors for the inner tracking system. Detectors with and without an additional layer of $Si_3N_4$ insulator were made in one set, using the same thickness of $SiO_2$ insulator. Measurements were made on both types of detectors after irradiation with 20 MeV electrons, using doses up to 2 Mrad. The additional $Si_3N_4$ layer allows a coupling capacitor breakdown voltage larger than 100 V and capacitor yield larger than 99 percent. However, the leakage current for detectors with double layer insulator is about 20 nA per strip while the leakage current for the single layer $SiO_2$ insulated detectors is only 0.5 nA. The 20 nA leakage current leads to 450 electrons noise when the ALICE 128C electronics with a peaking time of 1.4 microseconds is used. At a 1 nA leakage current the noise is 100 electrons. The ENC for an input capacitance of 5 pF is 300 electrons. Since all detectors show an increased leakage current after irradiation, the difference between the single and double layer insulation detectors becomes negligible when doses of the order of several hundreds of krad are applied.

## 2. Detector design

Since one plans to use in future the single-coordinate detector as a $p^+$-side of a two-coordinate detector, it is designed and manufactured with a large number of microstrip test structures, diodes and technological test structures (figure 1). The detector has been manufactured at SPA "Detector", Kiev, Ukraine.

### 1. 750 strips one-sided detector

The microstrip detector (figure 2) consists of 750 registering $p^+$ -strips with 100 μ m pitch. Strip width is 40 μ m, its length is 40 mm. The size of the sensitive zone of the microstrip detector is 40× 75 $mm^2$. The strips are

biased with integrated 1.5 MOhm polysilicon resistors. One is going to read out the information from the strips with the help of integrated coupling capacitors. To decrease and stabilize leakage currents, the microstrip detector is surrounded by guard rings. To protect against mechanical and chemical damage, the detector is coated with a passivating layer of silicon oxide. One opens up areas in the passivating layer only to Al contact pads of p-strips, coupling capacitors, guard rings and biasing line of integrated resistors.

## 2. Test microstrip structures

Simultaneously with the main microstrip detector, three microstrip test structures located at the edges of the plate have been manufactured. The first test microstrip structure is a single-sided microstrip detector with 64 $p^+$-strips loaded by integrated resistors. With the exception of the decreased number of strips the test structure corresponds to a full-scale detector. The microstrip test structure is provided for studying signal spectrum, space resolution and their variation under irradiation. In future it will be the $p^+$-side of a two-coordinate microstrip test structure.

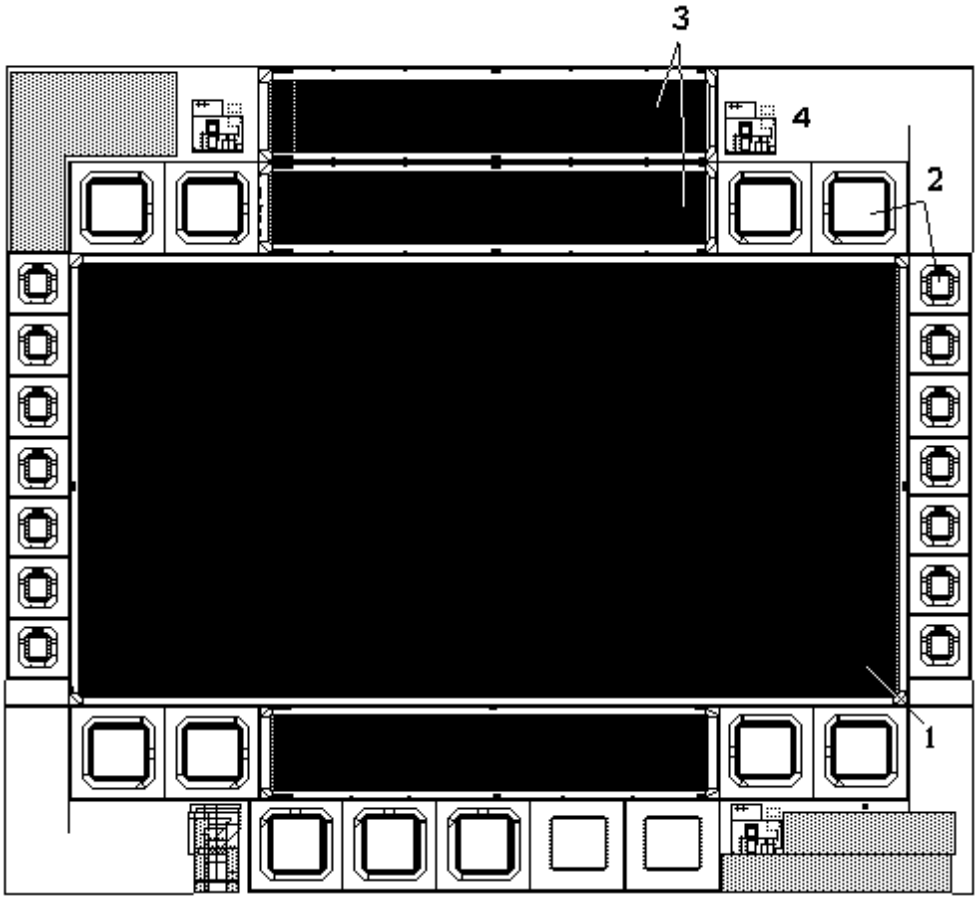

Fig.1. Wafer with microstrip detector (1) and test structures: 2- diodes, 3- microstrip test structures, 4- technological test structures.

The second test microstrip structure has been manufactured with the same number of strips but without integrated resistors. Such a structure is used for measuring interstrip resistance and other characteristics that can be measured only without integrated resistors.

The third test structure is manufactured as a plane detector with the $7\times 40$ $mm^2$ sensitive zone equal to sensitive zones of the first two test microstrip structures with 64 strips. On manufacturing a two-coordinate detector, this structure will be a single-sided $n^+$-microstrip detector.

All three test structures, like the main detector, are surrounded by guard rings and coated with a passivating layer.

### 2.3. Diode test structures

Microstrip detector and microstrip test structures are surrounded by diode test structures.

The diode test structures serve for studying the quality of silicon, for measuring the depleting voltage by a capacitive technique, for preliminary studies of the microstrip detector characteristics and evaluation of their behaviour under irradiation. Their application permits one to reduce the necessary number of microstrip detectors at the stage of research and development.

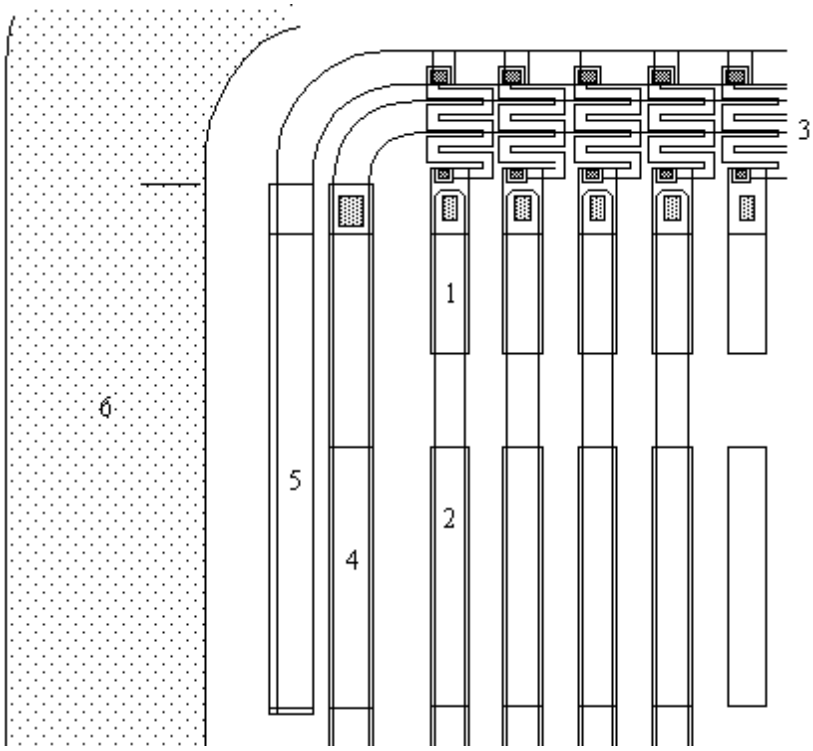


Fig.2. Microstrip detector corner: 1- DC pad, 2- AC pad, 3- polysilicon resistors, 4- $p^+$-guard ring, 5- basing pad, 6- $n^+$-guard ring.

The developed diode test structures may also be used in other applications like planar detectors and photo-diodes for applications in physics and medical practice.

The diode test structures are manufactured with sensitive zones of two sizes: $2\times 2$ mm$^2$ and $5\times 5$ mm$^2$. The size of the sensitive zone of the smaller diode structure corresponds to that of a single strip.

### 2.4. Technological test structures

Test structures are implemented on the wafer to monitor the technological process, for measuring the resistance of the layers of polysilicon, $p^+$- and $n^+$-implantations, for measuring contact resistance and other characteristics of the detector.

## 3. Processing of the prototypes

To manufacture the prototype of the $p^+$-side of a double-sided strip detector, one used four-inch wafers of n-silicon with resistivity of 3000-5000 Ohm·cm, <111> orientation and 350 μ m thick, polished from both sides.

In the process of the first oxidation a pyrogeneous oxide 0.3 μ m thick layer was grown at T=900 °C with addition of HCl. This oxide was used as a mask during ion implantation of phosphorus to form n+-guard rings. Phosphorus

ions with the energy E=60 keV and surface concentration $5\times 10^{14}$ at/cm$^2$ have been used. The backside has also been implanted with phosphorus to make the Ohmic contact but with a higher surface concentration of ions $2.5\times 10^{15}$ at/cm$^2$.

After the formation of $n^+$-rings, the protective oxide was removed and a new protective oxide 0.6 μ m thick was grown for masking during boron implantation. After formation of the pattern of $p^+$- regions, boron with the energy E=60 keV and surface concentration $5\times 10^{14}$ at/cm$^2$ was implanted. Phosphorus and boron ions were implanted through the layer of the dechanneling oxide 500 Å thick. After that, a $SiO_2$ layer 0.15 μ m thick was grown as the first layer of a two-layer capacitor dielectric. The layer of a high temperature $Si_3N_4$ 0.12 μ m thick was the second one. To perform a comparative analysis, the $Si_3N_4$ layer was not deposited on some of the plates.

To form the resistors, a film of polycrystalline silicon 0.55 μ m thick was deposited and doped by boron ion implantation up to the level required to obtain 1.5 MOhm resistors.

Contact holes to different layers ($p^+$, $n^+$ and polysilicon) were obtained by simultaneous wet etching the $SiO_2$ layers after lithographic formation of contact areas and plasma-chemical etching the $Si_3N_4$ layer in the region of contact areas.

Strip-detector metallisation was made by depositing Al with a small silicon admixture (1%). After lithographing aluminum, the passivating layer of the low temperature phosphorus-silicate glass 0.9 μ m thick was deposited that covered the total surface of the detector. The photolithography over the passivating layer opened only Al areas of contact pads for connections to the detector and test structures. The final annealing of the detector was made at T=400 ° C in hydrogen during 30 min.

Up to now two sets of detectors were produced. In the first set, only double-layer insulation was used to create the coupling capacitors. In the second set, the silicon nitride was not deposited on some of the wafers. In all other respects, all the second set wafers are identical, processed according to the same technological operations. Table 1 shows the characteristics of the produced single-coordinate microstrip detectors.

Fig. 3 shows the distribution of leakage currents and biasing resistor values for 750 strips detector with $Si_3N_4$ additional insulation.

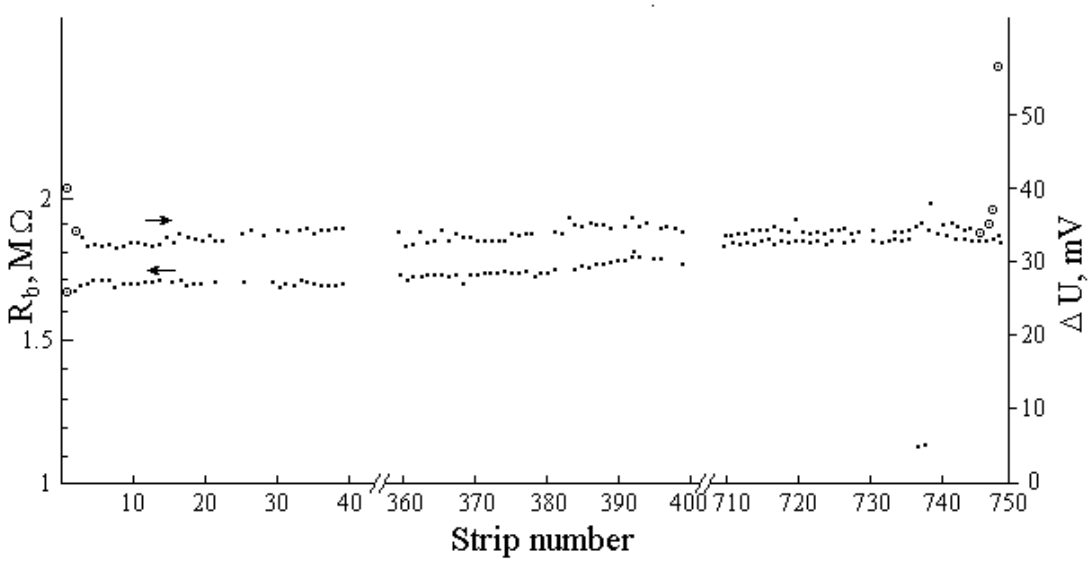


Fig.3. Leakage current (voltage on the integrated resistors) and integrated resistor value distributions for 750 strips detector.

**Table 1. Microstrip characteristics with and without $Si_3N_4$ insulation**

| 1996 set | | 1997 set | |
|---|---|---|---|
| | | I | II |
| Design | Ion implanted | The same | The same |
| | AC coupled structure | | |
| Technology | with polysilicon resistor | The same | The same |
| $Si_3N_4$ layer | and with oxide passivation | + | - |
| Active area | 4 inch silicon | The same | The same |
| No of channel | + | 750 | 750 |
| Pitch | 40× 75 $mm^2$ | 100 μ m | 100 μ m |
| Interstrip Capacitance | 750 | 4 pF | 4 pF |
| Interstrip Resistance | 100 μ m | | |

| | | | |
|---|---|---|---|
| Strip leakage<br>current (FD)<br>Biasing resistor<br>Coupling capacitors<br>Capacitor breakdown<br>Number of dead strips<br>on the leakage current<br>Number of broken<br>capacitors<br>Number of work. resistors | 4 pF<br>3<br>GOhm<br>20 nA<br>1.8 MOhm<br>200 pF<br>>100 V<br><1%<br><1%<br>100% | 3<br>GOhm<br>20 nA<br>1.5 MOhm<br>200 pF<br>>100 V<br><1%<br><1%<br>100% | 100<br>GOhm<br><1 nA<br>1.5 MOhm<br>300 pF<br>>25 V<br><1%<br><3%<br>100 % |

## 1. Test conditions

As is known, the action of radiation on semiconductor detectors is implemented, mainly, via two mechanisms. The first mechanism of bulk damaging consists in breaking the crystal symmetry through displacing atoms from their lattice sites. The second mechanism of surface damage consists in changing the charge state of the Si/SiO2 interface through the oxide ionization [1,2]. In view of this, to simulate the radiation conditions for the inner tracking system (ITS) of the ALICE detector, it is necessary to irradiate the detector with ~600 Gy of ionizing radiation and a neutron fluence of ~$10^{11}$ n/$cm^2$ (corresponding to 10 years of ALICE operation). Namely, the neutrons simulate the action of high energy particles on the bulk of the detector material [3,4].

The radiation tolerance of microstrip detectors in this paper was studies using 20 MeV electrons in the Kharkov Institute of Physics and Technology.

The absorbed dose (Gy) in the specimen irradiated with electrons was determined using the well-known values of ionization energy losses and the measured integral densities of electron fluxes. The absorbed dose and its distribution over the detector were also measured with color film dose meters. The color film-ref dose meters permit one to perform measurements with an accuracy • 20% under steady outer conditions and the temperature not exceeding 60$^{o}$C. The measurements

of the optical density of dose meters were made with micro-photometers.

### 4.1. Test of 20 MeV electrons bulk damaging efficiency

In the case of irradiation with high energy electrons, along with ionization, the action of electrons is determined by the generation of structure defects in the bulk of the crystal detector due to the displacement of substance atoms by accelerated electrons [1, 5, 6].

The efficiency of 20 MeV electron action on bulk material of the microstrip detector was determined from the change in the lifetime of charge carriers in silicon specimens-witnesses [ 5] . It is known that neglecting the influence of the surface one can determine the leakage current of a semiconductor detector from the relationship [7]

$$j=qn_jWA/2\tau , \qquad (1)$$

where q is the electron charge, W is the depth of the detector depletion, A is the active region of the detector, $\tau$ is the effective minority carrier lifetime and n is the intrinsic carrier concentration. The expression for change of the leakage current of the detector normalized by one acting particle or one dose unit will have the form

$$\Delta j= 0.5qn_jWA\cdot\Delta \tau^{-1}/D, \qquad (2)$$

similar to the well-known expression for the radiation constant of a semiconductor material [1]

$$K\tau =\Delta \tau^{-1}/D. \qquad (3)$$

Since the leakage current and the radiation constant of the detector material have similar dependencies on the carrier lifetime, then measuring the quantity $K\tau$ for the detector material, one can judge on the efficiency of radiation action on a semiconductor detectors. Measuring $K\tau$ was used in this paper for the determination of the relative efficiency of 20 MeV electrons required for the simulation of the action of 14 MeV neutrons with a given fluence on the bulk of the detector material. The measured data are given in Table 2.

**Table 2. Measurement of relative bulk damaging efficiency of 20 MeV and 3 MeV electrons, 14 MeV neutrons**

| Particle | Energy, MeV | Measured $K\tau$, $cm^2/s$ | $K\tau$ [1], $cm^2/s$ | Efficiency of electrons (relative to 14 MeV neutrons) |
|---|---|---|---|---|
| n | 14 | $1.5\cdot10^{-6}$ | $1.5–2\cdot10^{-6}$ | 1 |
| e | 3 | $1.5\cdot10^{-8}$ | $\sim2\cdot10^{-8}$ | 0.01 |
| e | 20 | $4.1\cdot10^{-8}$ | | 0.027 |

The results obtained for $K\tau$ for 3 MeV electrons and neutrons practically coincide with the results of the paper [1]. Using the efficiency value obtained we have assumed that the integral

flux of 20 MeV electrons 40 times exceeding the fluence of 14 MeV neutrons exerts on the detector characteristics the close action. We believe our procedure of irradiation to be valid taking into account the rather low radiation environment in ALICE. The predicted changes in the detector characteristics as a result of irradiation are not large. Correspondingly, the value of the inverse annealing of detector characteristics as a result of restructuring the bulk clusters of defects after irradiation [1, 8, 9] is negligible.

## 5. Results

The detector was irradiated in a non-biased state. The static characteristics of the detector were measured just after irradiation. For measuring static characteristics the probe stations developed and constructed at KhIPT were used. Now a miniature adapter is also developed and constructed to measure the characteristics of double-sided detectors before the readout electronics is mounted on them.

### 5.1. Depletion voltage

Fig. 4 shows the bulk capacity against the depletion voltage for different irradiation doses. The depletion voltage was studied with the capacitive technique [10] at 1 kHz and 1 MHz measuring frequency. The voltage of total depletion was determined from the point where the strong and weak variations of capacity against voltage in log-log coordinates intersect.

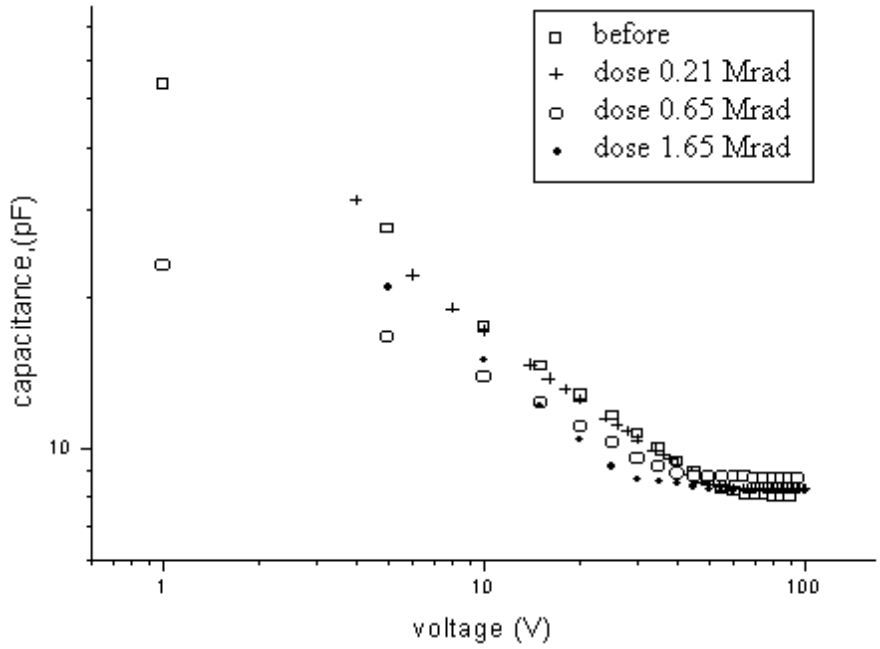


Fig.4. Bulk capacity against the bias voltage for different integral doses.

Fig. 5 shows the full depletion voltage against the irradiation dose. The changes of the full depletion voltage are slight for the doses expected in the ALICE experiment. One observes no change of the conductivity type in the range of doses under study.

### 5.2. Leakage currents

As one sees from Table 1, the detectors manufactured in one batch with silicon nitride, and without it exhibit different strip leakage currents, i.e., 20 nA and less than 1 nA, respectively. Perhaps, the increase of the leakage current for the detectors with the silicon nitride is associated with the increase of the surface generation-recombination centers on the open surface, and, especially, over the strip perimeter at the contact of the open surface and $p^+$-strip. The leakage current dependence on diode dimensions may support this viewpoint. Increasing the sensitive zone of the diode, the leakage current normalized by the unit of sensitive area decreases for diodes with $Si_3N_4$. Increasing the sensitive zone area, the ratio of the open surface of the detector (surface between the $p^+$-guard ring and p-implanted zone of the diode) to the sensitive area of the diode decreases. The ratio of the perimeter to the area of the sensitive zone also decreases. For the diodes without additional $Si_3N_4$ insulation layer the leakage currents normalized by the unit area are practically constant. Moreover, the value of the normalized current for the diode coincides with the one for the microstrip detector.

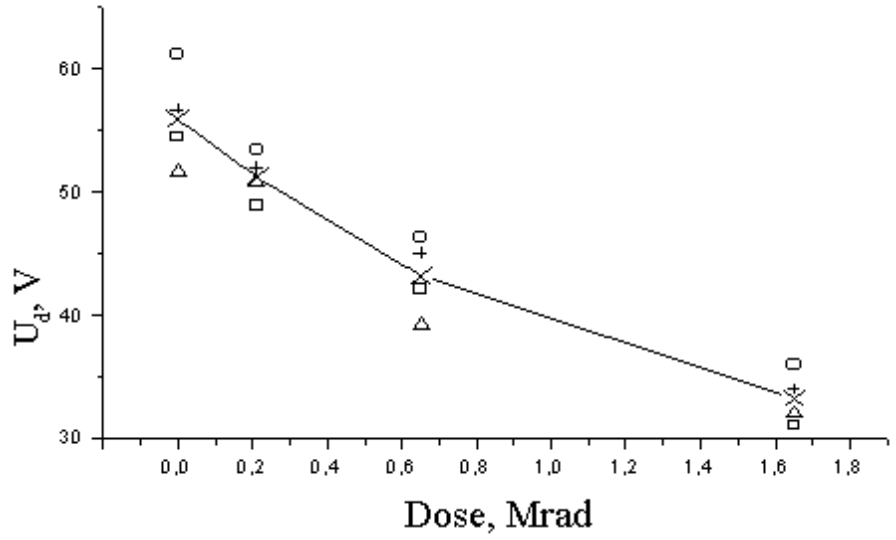


Fig.5. Full depletion voltage for different irradiation dose. O , □ , Δ , +– are here the data for four different detectors.

Fig. 6 shows the variation of leakage currents for microstrip detectors with and without $Si_3N_4$ under irradiation with 20 MeV electrons. One sees that these dependences are almost linear. Furthermore, the initial difference in current of ~20 nA observed for the detector with $Si_3N_4$ persists over the entire range of doses. It has to be pointed out that the large initial difference gets relatively much smaller at large irradiation doses. Fig. 7 shows the distribution of leakage currents for microstrip detectors with $Si_3N_4$ and without it before irradiation and after irradiation with the maximum dose. One sees that a good uniformity of the distribution of leakage currents persists after the maximum irradiation dose.

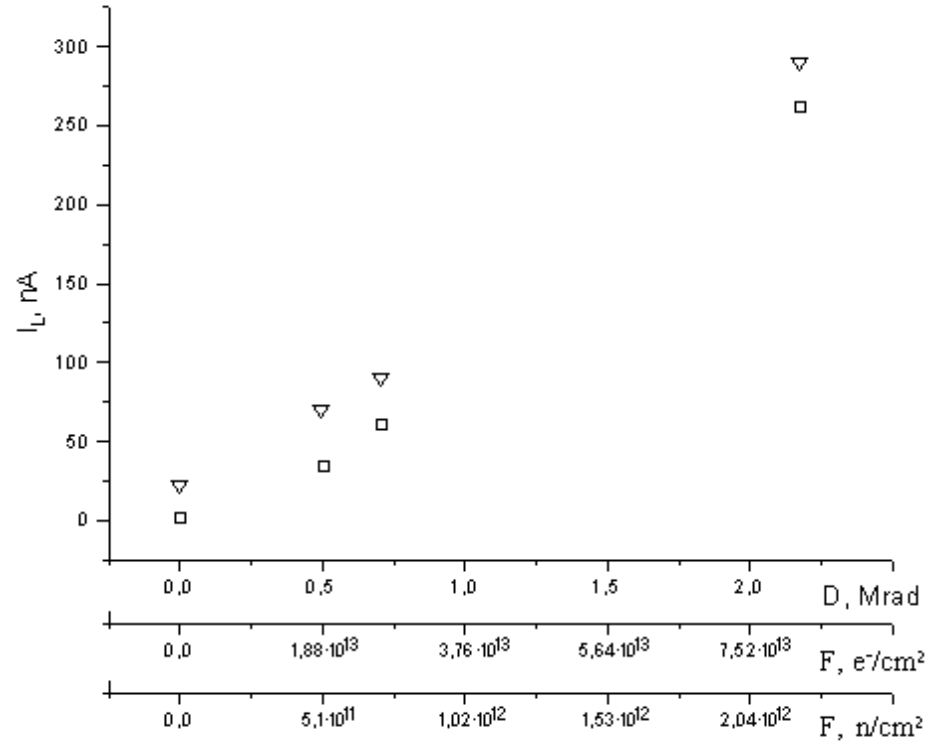


Fig.6. Leakage currents variation for microstrip detectors with (∇ ) and without $Si_3N_4$ (□ ).

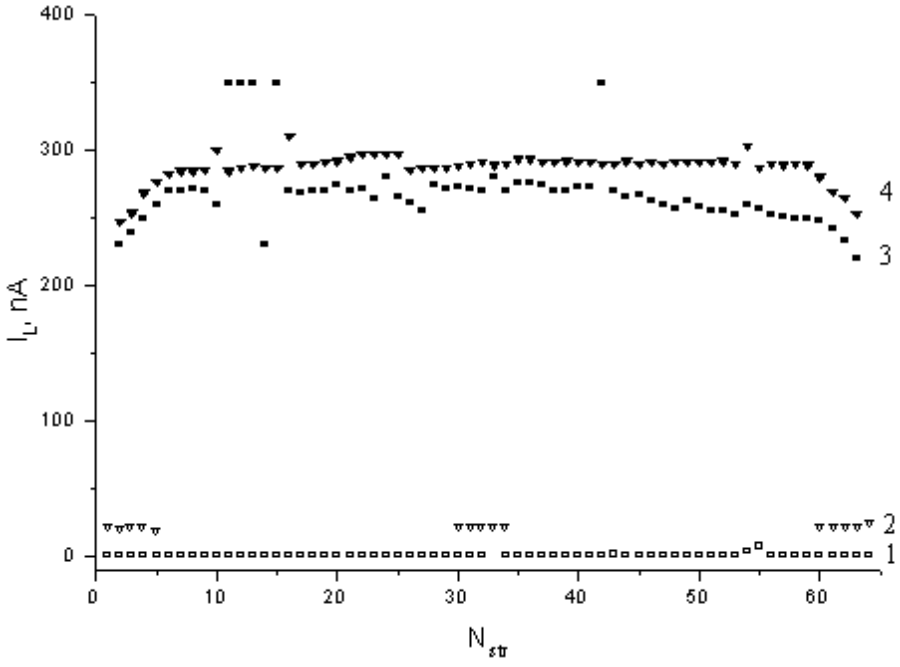


Fig.7. Leakage currents distributions before (1, 2) and after (3, 4) irradiation. 1, 3 single-layer and 2, 4 double-layer insulation.

### 5.3. Interstrip resistance

Fig. 8 shows the interstrip resistance for detectors with single-layer and double- layer insulation against irradiation dose. The same figure shows the variation of the ratio of interstrip resistances for the detectors with single-layer and double-layer insulation.

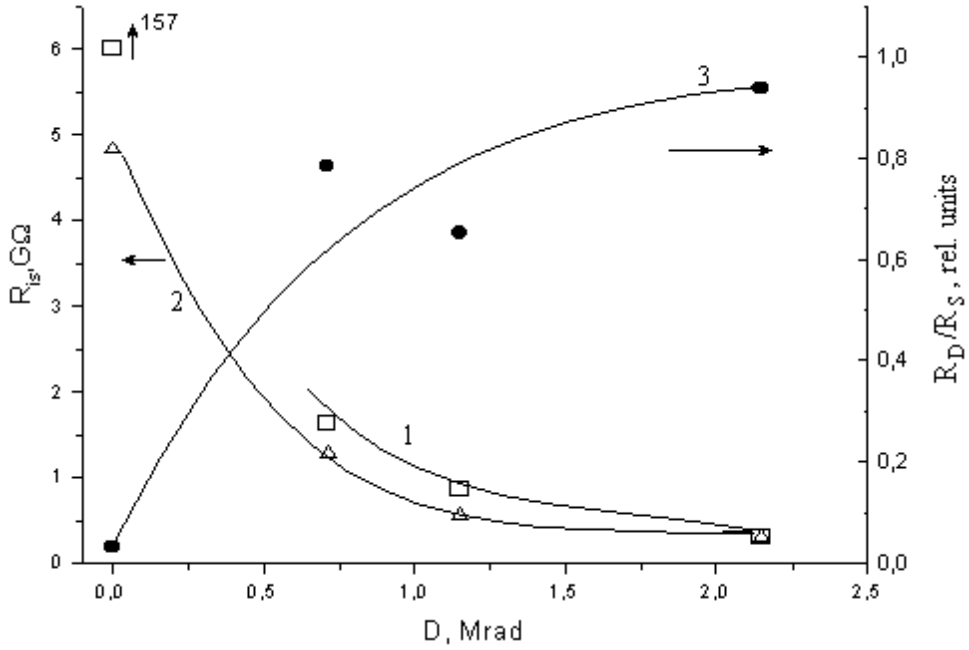


Fig.8. Interstrip resistance for the detectors without (1) and with (2) $Si_3N_4$. Interstrip resistances ratio for the detectors with double-layer and single-layer insulation (3).

Naturally, the surface conductivity, created by surface generation-recombination centers in the detectors with additional insulation, decreases the initial value of the interstrip resistance. However, one sees that the surface effect on the interstrip resistance also becomes insignificant already at irradiation doses <1 Mrad.

### 5.4. Interstrip and total strip capacitance

The large strip pitch (the strip pitch 100 μ m and interstrip gap 60 μ m) of the detector provides for small value of the interstrip and total strip capacitances. Perhaps, owing to the same reason, the interstrip capacity and total capacity of the strip show weak dependence on the irradiation dose.

### 6. Conclusions

In order to separate the leakage current of silicon microstrip detectors from the readout electronics capacitive coupling is used. The space needed for the capacitive coupling can be significantly reduced integrating the coupling capacitors on the detectors.

However, the standard use of $SiO_2$ as insulation layer for the capacitors limits the breakdown voltage of the capacitors. An additional insulation layer of $Si_3N_4$ significantly increases the breakdown voltage. Unfortunately, the use of $Si_3N_4$ also increases the leakage current of the detector.

It was shown that on single-sided silicon microstrip detectors on 4000 Ohm·cm n-type silicon the use of the $Si_3N_4$ insulation layer increased the leakage current from 1 nA/strip to 20 nA/strip. However, this increase in leakage current is small compared to the increase of leakage current induced by a less that 1 Mrad irradiation doses. After a 2 Mrad dose the leakage currents of both types of detectors were approximately 250 nA/strip.

**Acknowledgements**

The authors are very thankful to many colleagues for the valuable discussions and constructive remarks, especially P. Giubellino and O. Runolfsson. This work was supported by INTAS under the Grant 96-0678.

**References**

1. H.W. Kraner, Nucl. Instr. and Meth. A225, 1984, p. 616-618.
2. J. Kemmer and G. Lutz. Nucl. Instr. and Meth. A273, 1988, p. 588.
3. Technical Proposal for A Large Ion Collider Experiment at CERN LHC. CERN/LHCC/95-71, 15 December 1995.
4. A. Holmes-Siedle, M. Robbins, S Watts et al., Nucl. Instr. and Meth. A339, 1994, p. 511-523.
5. N. Maslov, G. Bochek, V. Kulibaba et. al., ALICE/95-19, Internal Note/SIL, 15 June 1995.
6. N.I. Maslov, G.D. Pugachev, M.I. Heifets. Physics and Technics of Semiconductors. Vol. 16, No 3, 1982, p. 513-515.
7. A.S. Grove, Physics and Technics of Semiconductor Devices, New York, Wiley, 1967, Ch. 6, p. 176-177.
8. I.D. Konozenko, A.K. Semenyuk and V.I. Khivrich, Radiation effects in semiconductors, eds., J.W. Corbett and G.D. Watkins, (Gordon and Breach, London, 1971).
9. E. Fretwurst, H. Feick, M. Glaser et al., Nucl. Instr. And Meth. A342 (1994), p. 119-125.
10. M. A. Frautschi et al., Capacitance Measurements of Double-Sided Silicon Microstrip Detectors, The New Mexico Center for Particle Physics CDF Collaboration note CDF/DOC/SEC_VTX/CDFR/2546.